

# Timelike vs spacelike DVCS from JLab, COMPASS to colliders and to ultraperipheral collisions at AFTER@LHC

Lech Szymanowski

Theoretical Physics Department  
National Center for Nuclear Research (NCBJ), Warsaw

Physics at A Fixed Target Experiment using the LHC beam  
ECT\*, Trento, 4-13 Feb. 2013

# Outline

- 1 Timelike Compton Scattering - Introduction
- 2 Basic properties of TCS, first experimental results
- 3 TCS at NLO
- 4 Ultraperipheral collisions
- 5 AFTER@LHC

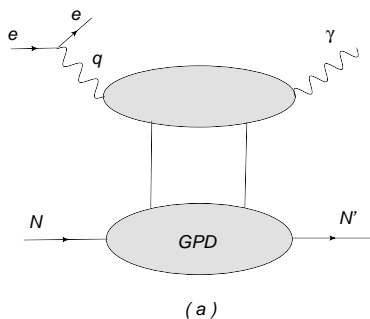


Figure: Deeply Virtual Compton Scattering :  $lN \rightarrow l'N'\gamma$

Skewness  $\xi$ :

$$\xi = -\frac{(P' - P)n}{(P + P')n}$$

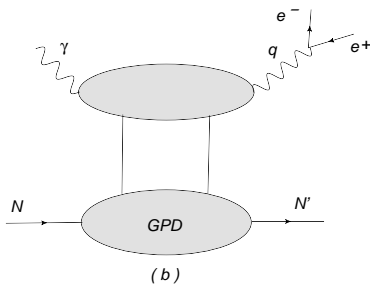


Figure: Timelike Compton Scattering:  $\gamma N \rightarrow l^+ l^- N'$

Skewness  $\eta$ :

$$\eta = -\frac{(P' - P)n}{(P + P')n}$$

## Why TCS?

- GPDs enter factorization theorems for hard exclusive reactions (DVCS, deeply virtual meson production, TCS etc.), in a similar manner as PDFs enter factorization theorem for DIS
- First moment of GPDs enters the Ji's sum rule for the angular momentum carried by partons in the nucleon,
- Deeply Virtual Compton Scattering (DVCS) is a golden channel for GPDs extraction,
- Why TCS: universality of the GPDs, spacelike-timelike crossing and understanding the structure of the NLO corrections,
- Experiments *at low energy*: CLAS 6 GeV  $\rightarrow$  CLAS 12 GeV, *at high energy*: COMPASS, RHIC, LHC and AFTER@LHC ?

## Coordinates

Berger, Diehl, Pire, 2002

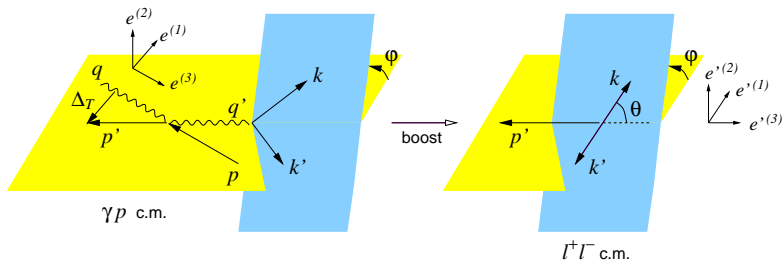


Figure: Kinematical variables and coordinate axes in the  $\gamma p$  and  $l^+ l^-$  c.m. frames.

## The Bethe-Heitler contribution

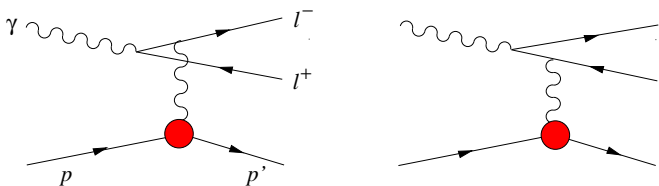
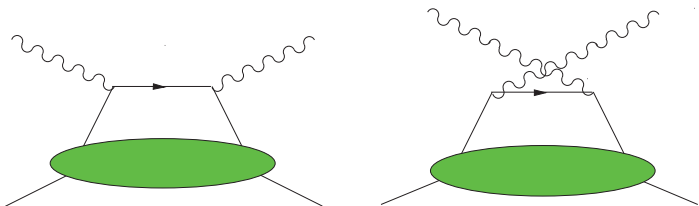


Figure: The Feynman diagrams for the Bethe-Heitler amplitude.

$$\frac{d\sigma_{BH}}{dQ'^2 dt d\cos\theta} \approx 2\alpha^3 \frac{1}{-tQ'^4} \frac{1 + \cos^2\theta}{1 - \cos^2\theta} \left( F_1(t)^2 - \frac{t}{4M_p^2} F_2(t)^2 \right),$$

For small  $\theta$  BH contribution becomes very large

# The Compton contribution



**Figure:** Handbag diagrams for the Compton process in the scaling limit.

$$\frac{d\sigma_{TCS}}{dQ'^2 d\Omega dt} \approx \frac{\alpha^3}{8\pi} \frac{1}{s^2} \frac{1}{Q'^2} \left( \frac{1 + \cos^2 \theta}{4} \right) 2(1 - \xi^2) |\mathcal{H}(\xi, t)|^2,$$

$$\mathcal{H}(\xi, t) = \sum_q e_q^2 \int_{-1}^1 dx T(x, \xi, Q') H^q(x, \xi, t),$$



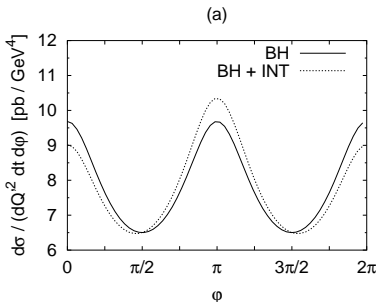
# Interference

The interference part of the cross-section for  $\gamma p \rightarrow \ell^+ \ell^- p$  with unpolarized protons and photons is given at leading order by

$$\frac{d\sigma_{INT}}{dQ'^2 dt d\cos\theta d\varphi} \sim \cos\varphi \operatorname{Re} \mathcal{H}(\xi, t)$$

Linear in GPD's, odd under exchange of the  $l^+$  and  $l^-$  momenta  $\Rightarrow$  angular distribution of lepton pairs is a good tool to study interference term.

Berger, Diehl, Pire, 2002



B-H dominant for small energies;

## JLAB 6 GeV data

Rafael Paredes PhD thesis

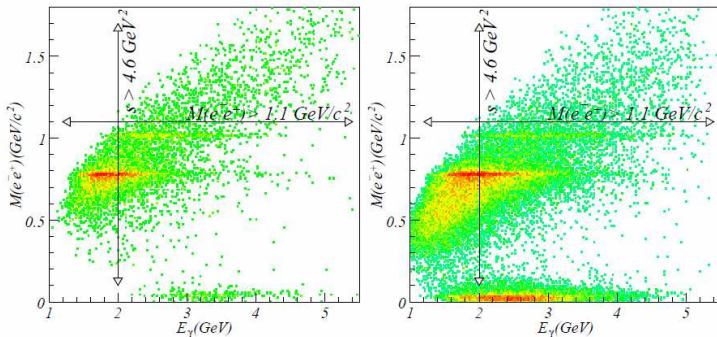


**Figure:**  $e^+e^-$  invariant mass distribution vs quasi-real photon energy. For TCS analysis  $M(e^+e^-) > 1.1 \text{ GeV}/c^2$  and  $s_{\gamma p} > 4.6 \text{ GeV}^2$  regions are chosen. Left graph represents e1-6 data set, right one is from e1f data set.

There is more data from g12 data set, soon to be analyzed. 12 GeV upgrade enables exploration of invariant masses up to  $Q^2 = 9 \text{ GeV}^2$  mass.

# Theory vs experiment

R.Paremuzyan and V.Guzey:

$$R = \frac{\int d\phi \cos\phi d\sigma}{\int d\phi d\sigma}$$

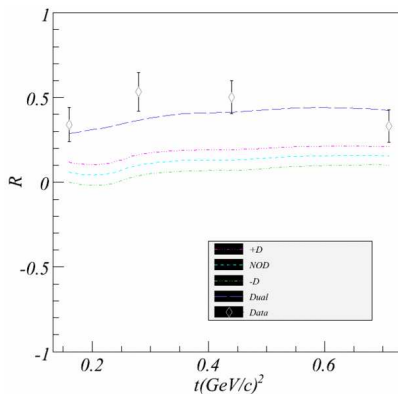


**Figure:** Theoretical prediction of the ratio  $R$  for various GPDs models. Data points after combining both e1-6 and e1f data sets.

# Motivation for NLO

Why do we need NLO corrections to TCS:

- gluons enter at NLO,
- DIS versus Drell-Yan: big K-factors
- reliability of the results, factorization scale dependence,

$$\log \frac{-Q^2}{\mu_F^2} \rightarrow \log \frac{Q^2}{\mu_F^2} \pm i\pi,$$

Belitsky, Mueller, Niedermeier, Schafer, Phys.Lett.B474 ,2000.

Pire, L.Sz., Wagner, Phys.Rev.D83, 2011.

General Compton Scattering:

$$\gamma^*(q_{in})N \rightarrow \gamma^*(q_{out})N'$$

- DVCS:  $q_{in}^2 < 0$ ,  $q_{out}^2 = 0$
- TCS:  $q_{in}^2 = 0$ ,  $q_{out}^2 > 0$
- DDVCS:  $q_{in}^2 < 0$ ,  $q_{out}^2 > 0$

## Amplitude:

$$\mathcal{A}^{\mu\nu} = -g_T^{\mu\nu} \int_{-1}^1 dx \left[ \sum_q^{n_F} T^q(x) F^q(x) + T^g(x) F^g(x) \right] \\ + i\epsilon_T^{\mu\nu} \int_{-1}^1 dx \left[ \sum_q^{n_F} \tilde{T}^q(x) \tilde{F}^q(x) + \tilde{T}^g(x) \tilde{F}^g(x) \right],$$

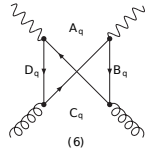
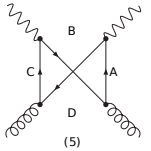
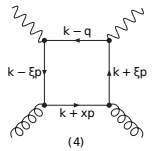
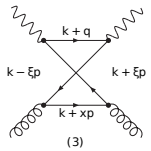
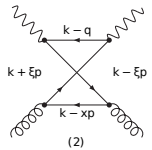
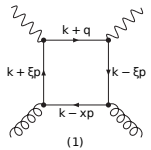
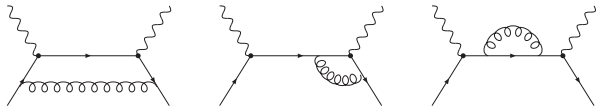
$$T^q(x) = \left[ C_0^q(x) + C_1^q(x) + \ln\left(\frac{Q^2}{\mu_F^2}\right) \cdot C_{coll}^q(x) \right] - (x \rightarrow -x),$$

$$T^g(x) = \left[ C_1^g(x) + \ln\left(\frac{Q^2}{\mu_F^2}\right) \cdot C_{coll}^g(x) \right] + (x \rightarrow -x),$$

$$\tilde{T}^q(x) = \left[ \tilde{C}_0^q(x) + \tilde{C}_1^q(x) + \ln\left(\frac{Q^2}{\mu_F^2}\right) \cdot \tilde{C}_{coll}^q(x) \right] + (x \rightarrow -x),$$

$$\tilde{T}^g(x) = \left[ \tilde{C}_1^g(x) + \ln\left(\frac{Q^2}{\mu_F^2}\right) \cdot \tilde{C}_{coll}^g(x) \right] - (x \rightarrow -x).$$

# Diagrams



## Results: TCS + DVCS + DDVCS

DVCS:

Quark coefficient functions:

$$C_0^q(x, \xi) = -e_q^2 \frac{1}{x + \xi - i\varepsilon},$$

$$C_1^q(x, \xi) = \frac{e_q^2 \alpha_S C_F}{4\pi} \frac{1}{x + \xi - i\varepsilon} \left[ 9 - 3 \frac{x + \xi}{x - \xi} \log\left(\frac{x + \xi}{2\xi} - i\varepsilon\right) - \log^2\left(\frac{x + \xi}{2\xi} - i\varepsilon\right) \right],$$

$$C_{coll}^q(x, \xi) = \frac{e_q^2 \alpha_S C_F}{4\pi} \frac{1}{x + \xi - i\varepsilon} \left[ -3 - 2 \log\left(\frac{x + \xi}{2\xi} - i\varepsilon\right) \right],$$

$$\tilde{C}_0^q(x, \xi) = -e_q^2 \frac{1}{x + \xi - i\varepsilon},$$

$$\tilde{C}_1^q(x, \xi) = \frac{e_q^2 \alpha_S C_F}{4\pi} \frac{1}{x + \xi - i\varepsilon} \left[ 9 - \frac{x + \xi}{x - \xi} \log\left(\frac{x + \xi}{2\xi} - i\varepsilon\right) - \log^2\left(\frac{x + \xi}{2\xi} - i\varepsilon\right) \right],$$

$$\tilde{C}_{coll}^q(x, \xi) = \frac{e_q^2 \alpha_S C_F}{4\pi} \frac{1}{x + \xi - i\varepsilon} \left[ -3 - 2 \log\left(\frac{x + \xi}{2\xi} - i\varepsilon\right) \right],$$

where  $C_F = (N_c^2 - 1)/(2N_c)$

## DVCS

Gluon coefficient functions:

$$C_1^g(x, \xi) = \frac{\Sigma e_q^2 \alpha_S T_F}{4\pi} \frac{1}{(x + \xi - i\varepsilon)(x - \xi + i\varepsilon)} \times \left[ 2 \frac{x + 3\xi}{x - \xi} \log \left( \frac{x + \xi}{2\xi} - i\varepsilon \right) - \frac{x + \xi}{x - \xi} \log^2 \left( \frac{x + \xi}{2\xi} - i\varepsilon \right) \right],$$

$$C_{coll}^g(x, \xi) = \frac{\Sigma e_q^2 \alpha_S T_F}{4\pi} \frac{2}{(x + \xi - i\varepsilon)(x - \xi + i\varepsilon)} \left[ -\frac{x + \xi}{x - \xi} \log \left( \frac{x + \xi}{2\xi} - i\varepsilon \right) \right],$$

$$\tilde{C}_1^g(x, \xi) = \frac{\Sigma e_q^2 \alpha_S T_F}{4\pi} \frac{1}{(x + \xi - i\varepsilon)(x - \xi + i\varepsilon)} \times \left[ -2 \frac{3x + \xi}{x - \xi} \log \left( \frac{x + \xi}{2\xi} - i\varepsilon \right) + \frac{x + \xi}{x - \xi} \log^2 \left( \frac{x + \xi}{2\xi} - i\varepsilon \right) \right],$$

$$\tilde{C}_{coll}^g(x, \xi) = \frac{\Sigma e_q^2 \alpha_S T_F}{4\pi} \frac{2}{(x + \xi - i\varepsilon)(x - \xi + i\varepsilon)} \left[ \frac{x + \xi}{x - \xi} \log \left( \frac{x + \xi}{2\xi} - i\varepsilon \right) \right],$$

where  $T_F = \frac{1}{2}$



## Discussion

D. Mueller, B. Pire, L. Sz. and J. Wagner, Phys. Rev. D 86

The relation between the coefficient functions for NLO DVCS and NLO TCS:

$$\begin{aligned} TCS_{T^q} &= DVCS_{T^q}^* - i\pi^{DVCS} C_{coll}^{q*} \\ TCS_{T^g} &= DVCS_{T^g}^* - i\pi^{DVCS} C_{coll}^{g*} . \end{aligned}$$

## Models for GPDs

Double distribution + D-term

Müller 94, Ji 97, Radyushkin 97,  
Polyakov, Weiss 99

$$F_i(x, \xi, t) = \int_{-1}^1 d\beta \int_{-1+|\beta|}^{1-|\beta|} d\alpha \delta(\beta + \xi\alpha - x) f_i(\beta, \alpha, t) + D_i^F \left( \frac{x}{\xi}, t \right) \Theta(\xi^2 - x^2),$$

 $f_i(\beta, \alpha, t)$  - double distribution (DD) $D_i^F \left( \frac{x}{\xi}, t \right)$  - D-term

- the polynomiality (Lorentz inv.) of the Mellin moments satisfied automatically

## Models for GPDs

Double distribution + D-term

Müller 94, Ji 97, Radyushkin 97,  
Polyakov, Weiss 99

$$F_i(x, \xi, t) = \int_{-1}^1 d\beta \int_{-1+|\beta|}^{1-|\beta|} d\alpha \delta(\beta + \xi\alpha - x) f_i(\beta, \alpha, t) + D_i^F \left( \frac{x}{\xi}, t \right) \Theta(\xi^2 - x^2),$$

- the polynomiality (Lorentz inv.) of the Mellin moments satisfied automatically
- models for DD  $f_i(\beta, \alpha, t)$ :

$$f_i(\beta, \alpha, t) = g_i(\beta, t) h_i(\beta) \frac{\Gamma(2n_i + 2)}{2^{2n_i+1} \Gamma^2(n_i + 1)} \frac{[(1 - |\beta|)^2 - \alpha^2]^{n_i}}{(1 - |\beta|)^{2n_i+1}},$$

the profile function  $h_i(\beta)$  related to forward PDF e.g.  $h_{\text{val}}^q(\beta) = q_{\text{val}}(\beta) \Theta(\beta)$

$g_i(\beta, t)$  controls  $t$ -dependence of GPDs

## Models for GPDs

Our predictions are based on two models of GPDs:

- Goloskokov-Kroll (GK) model

CTEQ6m PDFs and Regge type  $t$ -dependence  $g_i(\beta, t) = e^{b_i t} |\beta|^{-\alpha'_i t}$

- model based on MSTW08 PDFs and on nucleon e-m. FFs

$$\begin{aligned} g_u(\beta, t) &= \frac{1}{2} F_1^u(t), \\ g_d(\beta, t) &= F_1^d(t), \\ g_s(\beta, t) &= g_g(\beta, t) = F_D(t), \end{aligned}$$

where

$$\begin{aligned} F_1^u(t) &= 2F_1^p(t) + F_1^n(t), \\ F_1^d(t) &= F_1^p(t) + 2F_1^n(t), \\ F_D(t) &= (1 - t/M_V^2)^{-2}, \end{aligned}$$

H. Moutarde, B. Pire, F. Sabatie, L.Sz. and J. Wagner, "On timelike and spacelike deeply virtual Compton scattering at next to leading order," arXiv:1301.3819

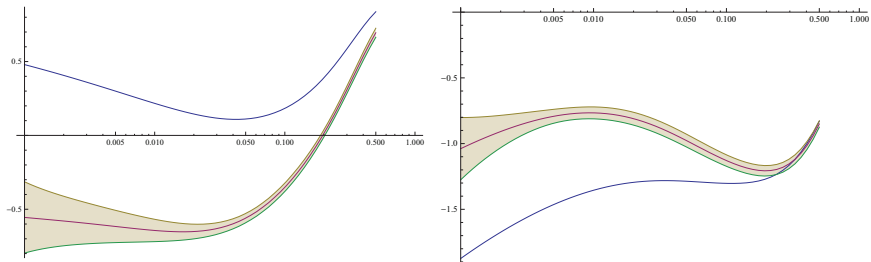


**Figure:** The real (left) and imaginary(right) parts of the TCS Compton Form Factor  $\mathcal{H}$  multiplied by  $\xi$ , as a function of  $\xi$  in the double distribution model based on MSTW08 parametrization, for  $\mu_F^2 = Q^2 = 4 \text{ GeV}^2$  and  $t = -0.1 \text{ GeV}^2$ . The shaded bands show the effect of a one sigma uncertainty of the input MSTW08 fit to the parton distributions.

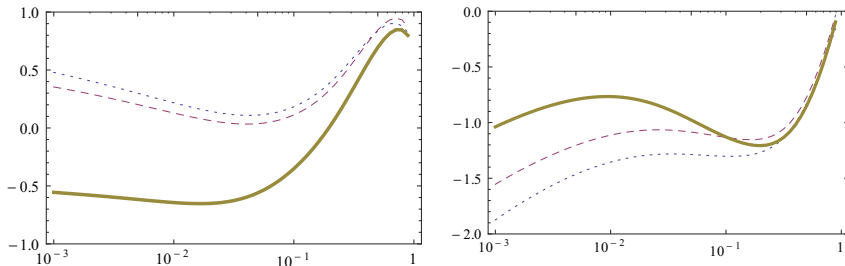


**Figure:** The real (left) and imaginary(right) parts of the TCS Compton Form Factor  $\mathcal{H}$  multiplied by  $\xi$ , as a function of  $\xi$  in the double distribution model based on MSTW08 parametrization, for  $\mu_F^2 = Q^2 = 4 \text{ GeV}^2$  and  $t = -0.1 \text{ GeV}^2$ .

LO : dotted line

LO + NLO-quark : dashed line

LO + NLO-quark + NLO-gluon: solid line

TCS:

GK

vs

MSTW

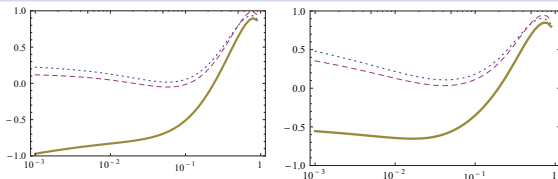


**Figure:** The real parts of the TCS Compton Form Factor  $\mathcal{H}$  multiplied by  $\xi$ , as a function of  $\xi$  in the double distribution model, for  $\mu_F^2 = Q^2 = 4 \text{ GeV}^2$  and  $t = -0.1 \text{ GeV}^2$ . GK- left figure, MSTW- right figure

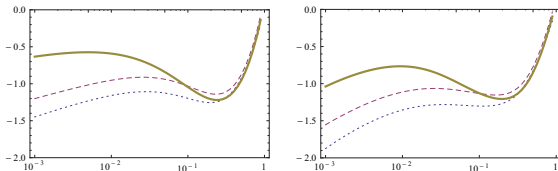


**Figure:** The imaginary parts of the TCS Compton Form Factor  $\mathcal{H}$  multiplied by  $\xi$ , as a function of  $\xi$  in the double distribution model, for  $\mu_F^2 = Q^2 = 4 \text{ GeV}^2$  and  $t = -0.1 \text{ GeV}^2$ . GK- left figure, MSTW- right figure

LO: dotted line

LO + NLO-quark: dashed line

LO + NLO-quark + NLO-gluon: solid line

## Observables

These CFFs are the GPD dependent quantities which enter the scattering amplitudes

For DVCS they are defined as

$$\mathcal{A}^{\mu\nu}(\xi, t) = -e^2 \frac{1}{(P+P')_+} \bar{u}(P') \left[ g_T^{\mu\nu} \left( \mathcal{H}(\xi, t) \gamma^+ + \mathcal{E}(\xi, t) \frac{i\sigma^{+\rho} \Delta_\rho}{2M} \right) + i\epsilon_T^{\mu\nu} \left( \tilde{\mathcal{H}}(\xi, t) \gamma^+ \gamma_5 + \tilde{\mathcal{E}}(\xi, t) \frac{\Delta^+ \gamma_5}{2M} \right) \right] u(P)$$

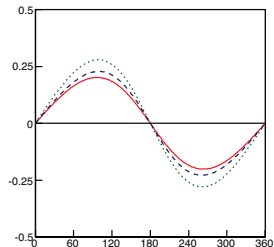
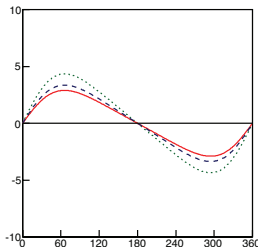
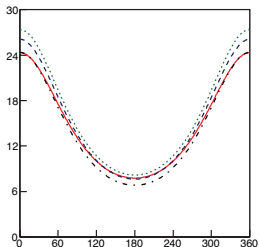
Similar relation holds for TCS with  $\xi$  replaced by  $\eta$ .



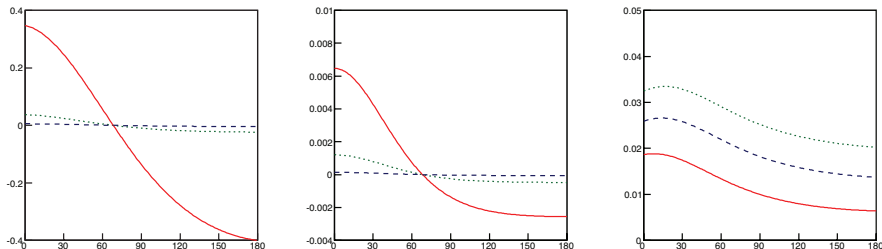
$$d\sigma(l_+) + d\sigma(l_-)$$

$$d\sigma(l_-) - d\sigma(l_+)$$

Asymmetry



**Figure:** From left to right, the total DVCS cross section in  $\text{pb}/\text{GeV}^4$ , the difference of cross sections for opposite lepton helicities in  $\text{pb}/\text{GeV}^4$ , the corresponding asymmetry, all as a function of the usual  $\phi$  angle (in Trento conventions) for  $E_e = 11 \text{ GeV}$ ;  $\mu_F^2 = Q^2 = 4 \text{ GeV}^2$  and  $t = -0.2 \text{ GeV}^2$ . The GPD  $H(x; \xi; t)$  is parametrized by the GK model. The contributions from other GPDs are not included. The Bethe-Heitler contribution appears as the dash-dotted line in the cross section plots (left part)

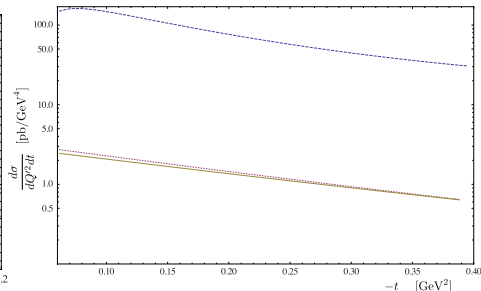
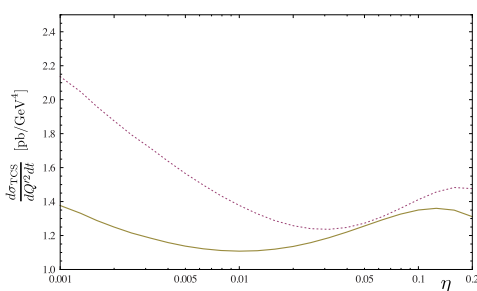


**Figure:** From left to right: mixed charge-spin asymmetry, mixed charge-spin difference and mixed charge-spin sum. The kinematical point is chosen as  $\xi = 0.05$ ,  $Q^2 = 4 \text{ GeV}^2$ ,  $-t = 0.2 \text{ GeV}^2$ . The GPD  $H(x; \xi; t)$  is parametrized by the GK model. The contributions from other GPDs are not included.

$$\mathcal{A}_{CS,U}(\phi) \equiv \frac{\mathcal{D}_{CS,U}}{\mathcal{S}_{CS,U}}, \quad \mathcal{D}_{CS,U}(\phi) \equiv d\sigma^{\rightarrow} - d\sigma^{\leftarrow}, \quad \mathcal{S}_{CS,U}(\phi) \equiv d\sigma^{\rightarrow} + d\sigma^{\leftarrow}$$

LO: dotted line      LO + NLO-quark: dashed line      LO + NLO-quark + NLO-gluon: solid line

Cross-section:

fixed  $t = -0.2 \text{ GeV}^2$ fixed  $\eta = 0.11$ 

**Figure:** left : LO (dotted) and NLO (solid) the TCS contribution to the cross-section as a function of  $\eta$  for  $Q^2 = \mu^2 = 4 \text{ GeV}^2$ , and  $t = -0.2 \text{ GeV}^2$  integrated over  $\theta \in (\pi/4, 3\pi/4)$  and over  $\phi \in (0, 2\pi)$ . Right : LO (dotted) and NLO (solid) TCS and Bethe-Heitler (dashed) contributions to the cross-section as a function of  $t$  for  $Q^2 = \mu^2 = 4 \text{ GeV}^2$  integrated over  $\theta \in (\pi/4, 3\pi/4)$  and over  $\phi \in (0, 2\pi)$  for  $E_\gamma = 10 \text{ GeV}$  ( $\eta \approx 0.11$ ).

large BH  $\Rightarrow$  need for more differential observables

Azimuthal-dependent cross-section:

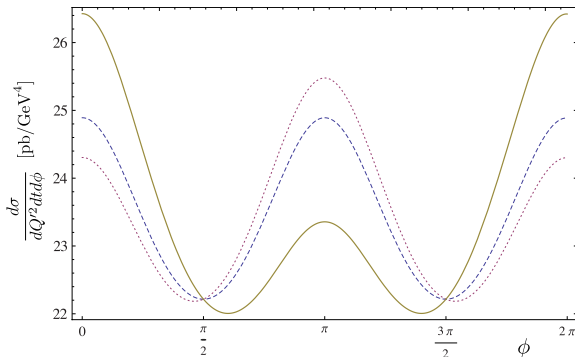


**Figure:** The  $\phi$  dependence of the cross-section at  $E_\gamma = 10$  GeV,  $Q^2 = \mu^2 = 4$  GeV<sup>2</sup>, and  $t = -0.1$  GeV<sup>2</sup> integrated over  $\theta \in (\pi/4, 3\pi/4)$ : pure Bethe-Heitler contribution (dashed), Bethe-Heitler plus interference contribution at LO (dotted) and NLO (solid).

Observable linear in  $Re\mathcal{H}$ : $dS \sim d\sigma$ 

$$R(\eta) = \frac{2 \int_0^{2\pi} d\phi \cos\phi \frac{dS}{dQ^2 dt d\phi}}{\int_0^{2\pi} d\phi \frac{dS}{dQ^2 dt d\phi}}$$

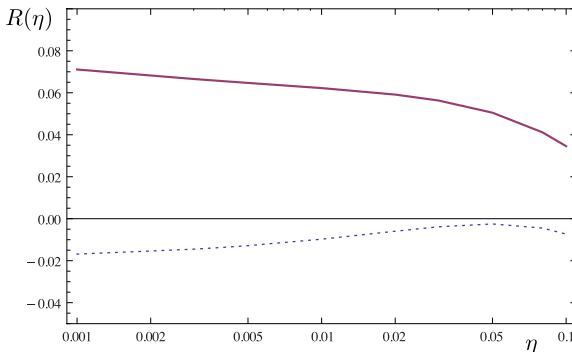
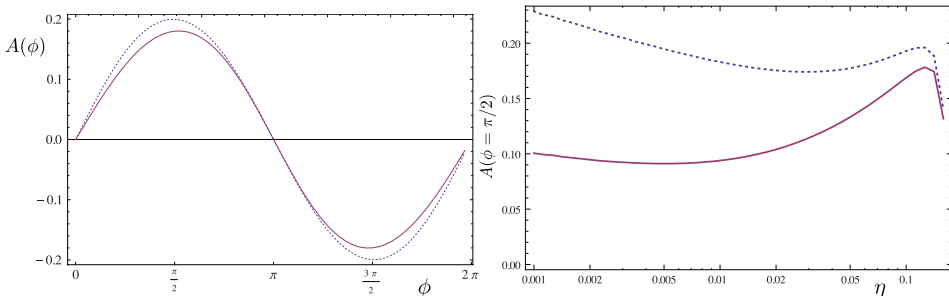


Figure: Ratio  $R$  as a function of  $\eta$ , for  $Q^2 = \mu_F^2 = 4 \text{ GeV}^2$  and  $t = -0.1 \text{ GeV}^2$ . The dotted line represents LO contribution and the solid line represents NLO result.

The measure of  $Im\mathcal{H}$ :

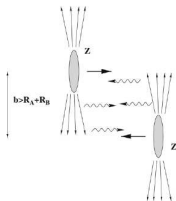
the photon beam circular polarization asymmetry

$$A = \frac{\sigma^+ - \sigma^-}{\sigma^+ + \sigma^-}$$



**Figure:** (left) Photon beam circular polarization asymmetry as a function of  $\phi$ , for  $t = -0.1 \text{ GeV}^2$ ,  $Q^2 = \mu^2 = 4 \text{ GeV}^2$ , integrated over  $\theta \in (\pi/4, 3\pi/4)$  and for  $E_\gamma = 10 \text{ GeV}^2$  ( $\eta \approx 0.11$ ). (right) The  $\eta$  dependence of the photon beam circular polarization asymmetry for  $Q^2 = \mu^2 = 4 \text{ GeV}^2$ , and  $t = -0.2 \text{ GeV}^2$  integrated over  $\theta \in (\pi/4, 3\pi/4)$ . The LO result is shown as the dotted line, the full NLO result by the solid line.

## Ultraperipheral collisions



$$\sigma_{pp} = 2 \int \frac{dn(k)}{dk} \sigma_{\gamma p}(k) dk$$

$\sigma_{\gamma p}(k)$  is the cross section for the  $\gamma p \rightarrow pl^+l^-$  process and  $k$  is the  $\gamma$ 's energy, and  $\frac{dn(k)}{dk}$  is an equivalent photon flux.

For  $\theta = [\pi/4, 3\pi/4]$ ,  $\phi = [0, 2\pi]$ ,  $t = [-0.05 \text{ GeV}^2, -0.25 \text{ GeV}^2]$ ,  $Q'^2 = [4.5 \text{ GeV}^2, 5.5 \text{ GeV}^2]$ , and photon energies  $k = [20, 900] \text{ GeV}$  we get:

$$\sigma_{pp}^{BH} = 2.9 \text{ pb} .$$

The Compton contribution gives:

$$\sigma_{pp}^{TCS} = 1.9 \text{ pb} .$$

## The interference cross section

B. Pire, L.Sz, J. Wagner (b), Phys. Rev. D 2009

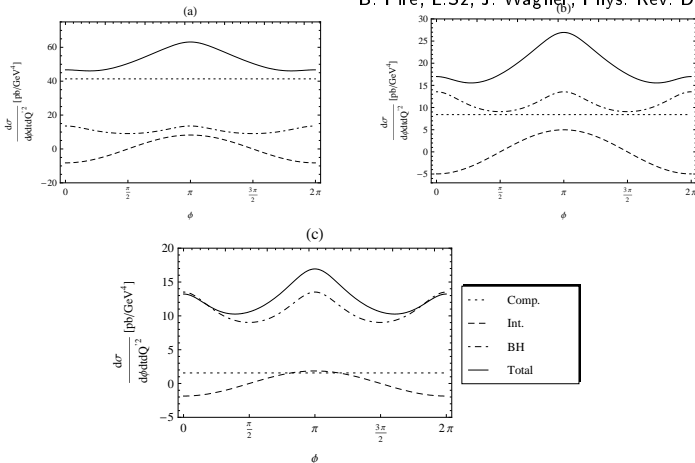


**Figure:** The differential cross sections (solid lines) for  $t = -0.2 \text{ GeV}^2$ ,  $Q'^2 = 5 \text{ GeV}^2$  and integrated over  $\theta = [\pi/4, 3\pi/4]$ , as a function of  $\varphi$ , for  $s = 10^7 \text{ GeV}^2$  (a),  $s = 10^5 \text{ GeV}^2$  (b),  $s = 10^3 \text{ GeV}^2$  (c) with  $\mu_F^2 = 5 \text{ GeV}^2$ . We also display the Compton (dotted), Bethe-Heitler (dash-dotted) and Interference (dashed) contributions.



## Ultraperipheral collisions at RHIC

$$L \cdot k \frac{dn}{dk} (\text{mb}^{-1} \text{sec}^{-1})$$

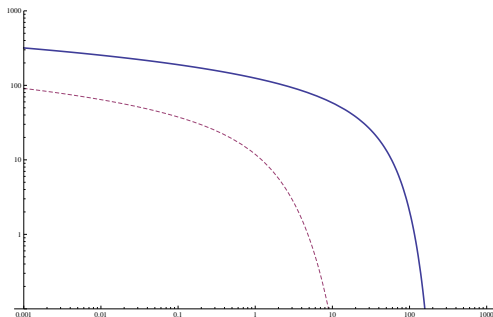


**Figure:** Effective luminosity of the photon flux from the Au-Au (dashed) and proton-proton (solid) collisions as a function of photon energy  $k$ (GeV).

$$\frac{d\sigma^{AuAu}}{dQ^2 dt d\phi} (\mu\text{b GeV}^{-4})$$

J. Wagner

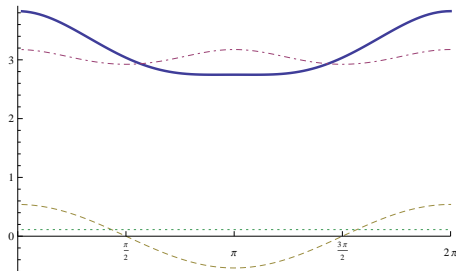


**Figure:** The differential cross sections (solid lines) for  $t = -0.1 \text{ GeV}^2$ ,  $Q'^2 = 5 \text{ GeV}^2$  and integrated over  $\theta = [\pi/4, 3\pi/4]$ , as a function of  $\phi$ . We also display the Compton (dotted), Bethe-Heitler (dash-dotted) and Interference (dashed) contributions.

Total BH cross section (for  $Q \in (2, 2.9) \text{ GeV}$ ,  $t \in (-0.2, -0.05) \text{ GeV}^2$ ,  $\theta = [\pi/4, 3\pi/4]$  and  $\phi \in (0, 2\pi)$ )

$$\sigma_{BH} = 41 \mu\text{b}$$

$$\text{Rate} = 0.04 \text{ Hz}$$

## Ultraperipheral scattering with A Fixed-Target Experiment at the LHC

## Ultrapерipheral scattering with A Fixed-Target Experiment at the LHC

### Motivation for AFTER@LHC:

“A Fixed-Target Experiment at the LHC (AFTER@LHC) : luminosities, target polarisation and a selection of physics studies,” PoS QNP (2012) 049 [arXiv:1207.3507 [hep-ex]]

“Ultra-relativistic heavy-ion physics with AFTER@LHC,” arXiv:1211.1294 [nucl-ex]

A. Rakotozafindrabe<sup>a</sup>, R. Arnaldi<sup>b</sup>, S.J. Brodsky<sup>c</sup>, V. Chambert<sup>d</sup>, J.P. Didelez<sup>d</sup>, B. Genolini<sup>d</sup>, E.G. Ferreira<sup>e</sup>, F. Fleuret<sup>f</sup>, C. Hadjidakis<sup>d</sup>, J.P. Lansberg<sup>d</sup>, P. Rosier<sup>d</sup>, I. Schienbein<sup>g</sup>, E. Scomparin<sup>b</sup>, U.I. Uggerhøj<sup>h</sup>

<sup>a</sup> IRFU/SPhN, CEA Saclay, 91191 Gif-sur-Yvette Cedex, France

<sup>b</sup> INFN Sez. Torino, Via P. Giuria 1, I-10125, Torino, Italy

<sup>c</sup> SLAC National Accelerator Laboratory, Theoretical Physics, Stanford U., Menlo Park, CA 94025, USA

<sup>d</sup> IPNO, Université Paris-Sud, CNRS/IN2P3, F-91406, Orsay, France

<sup>e</sup> Departamento de Física de Partículas, Universidad de Santiago de C., 15782 Santiago de C., Spain

<sup>f</sup> Laboratoire Leprince Ringuet, École Polytechnique, CNRS/IN2P3, 91128 Palaiseau, France

<sup>g</sup> LPSC, Université Joseph Fourier, CNRS/IN2P3/INPG, F-38026 Grenoble, France

<sup>h</sup> Department of Physics and Astronomy, University of Aarhus, Denmark

J. Ph. Lansberg, L.Sz. and J. Wagner

Case A : proton beam on lead (Pb) target,  $\sqrt{s} = 115 \text{ GeV}$ ,  $\epsilon = 1$ Case B : lead (Pb) beam on proton target,  $\sqrt{s} = 72 \text{ GeV}$ ,  $\epsilon = -1$ 

$$p = \frac{\sqrt{s}}{2} (1, 0, 0, \epsilon\alpha)$$

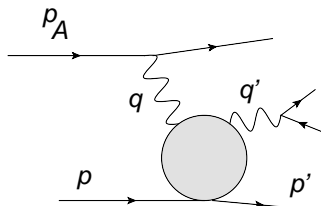
$$p_A = \frac{\sqrt{s}}{2} (1, 0, 0, -\epsilon\alpha)$$

$$q = x_\gamma \frac{\sqrt{s}}{2} (1, 0, 0, -\epsilon)$$

$$q' = (q'_0, q'_\perp, q'_z)$$

$$p' = (p'_0, p'_\perp, p'_z)$$

$$\text{where } \alpha = \sqrt{1 - \frac{4M^2}{s}}$$



Flux of  $\gamma$ 's:

Baltz et al, Phys. Rep. 458

$$\frac{dn}{dx_\gamma} = \frac{2Z^2\alpha_{EM}}{\pi x_\gamma} \left[ \omega^{pA} K_0(\omega^{pA}) K_1(\omega^{pA}) - \frac{\omega^{pA^2}}{2} \left( K_1^2(\omega^{pA}) - K_0^2(\omega^{pA}) \right) \right]$$

where:  $\omega^{pA} = x_\gamma M_p (r_p + R_A)$ .

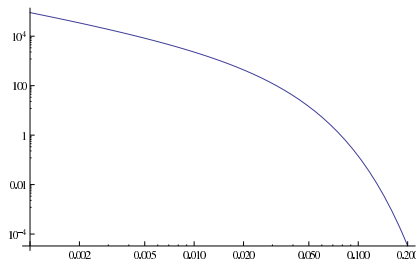


Figure:  $\frac{dn}{dx_\gamma}$

Rapidity of the outgoing photon::

$$y = \frac{1}{2} \log \frac{q'_0 + q'_z}{q'_0 - q'_z} = \epsilon \frac{1}{2} \log \left[ \frac{(Q^2 - t)(\alpha + 1)}{Q^2(\alpha - 1) - t(\alpha - 1 - 2x) + sx_\gamma^2(\alpha + 1)} \right]$$

Inverting we get:

$$\frac{dx_\gamma}{dy} = \frac{(-2\epsilon)(Q^2 - t)(\alpha + 1)e^{-2\epsilon y}}{\sqrt{4t^2 - 4s(Q^2 - t)(\alpha + 1) ((\alpha - 1) - (\alpha + 1)e^{-2\epsilon y})}}$$

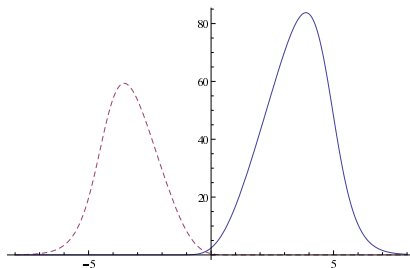


Figure:  $\left| \frac{dn}{dy} \right|$ , Case A (solid) and case B (dashed).

We consider Bethe-Heitler, TCS, and Interference term.

They are functions of  $s_{p\gamma}$ ,  $t$ ,  $Q$ ,  $\phi$ ,  $\theta$ .

We integrate over  $\theta \in (\pi/4, 3\pi/4)$ , in the region where the TCS/BH is the best seen.

Case A (p beam on Pb target):

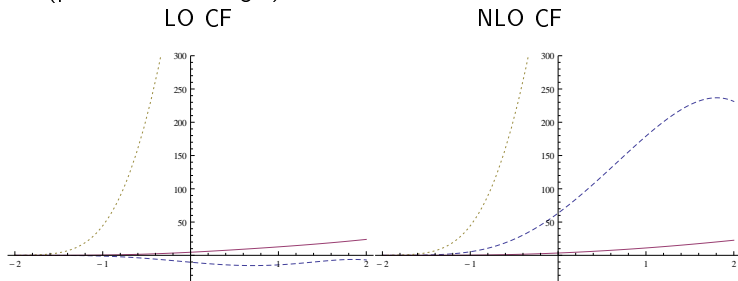


Figure:  $\frac{d\sigma}{dQ^2 dt dy d\phi}$  in  $pb/\text{GeV}^4$  for BH(dotted), TCS(solid), Interference(dashed) as a function of  $y$  (in CMS) for  $Q^2 = 4 \text{ GeV}^2$ ,  $t = -0.1 \text{ GeV}^2$ ,  $\phi = 0$ .



We consider Bethe-Heitler, TCS, and Interference term.

They are functions of  $s_{p\gamma}$ ,  $t$ ,  $Q$ ,  $\phi$ ,  $\theta$ .

We integrate over  $\theta \in (\pi/4, 3\pi/4)$ , in the region where the TCS/BH is the best seen.

Case A (p beam on Pb target):

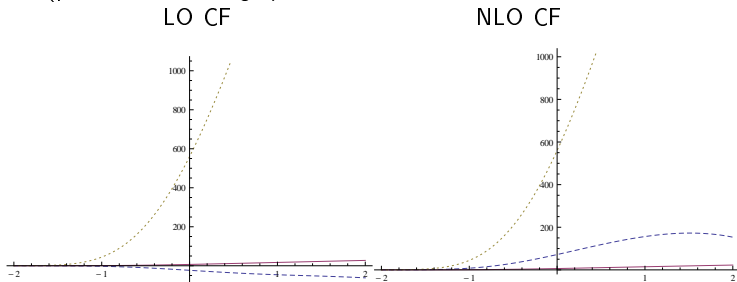


Figure:  $\frac{d\sigma}{dQ^2 dt dy d\phi}$  in  $pb/\text{GeV}^4$  for BH(dotted), TCS(solid), Interference(dashed) as a function of  $y$  (in CMS) for  $Q^2 = 4\text{ GeV}^2$ ,  $t = -0.1\text{ GeV}^2$ ,  $\phi = 0$ .

We consider Bethe-Heitler, TCS, and Interference term.

They are functions of  $s_{p\gamma}$ ,  $t$ ,  $Q$ ,  $\phi$ ,  $\theta$ .

We integrate over  $\theta \in (\pi/4, 3\pi/4)$ , in the region where the TCS/BH is the best seen.

Case A (p beam on Pb target):

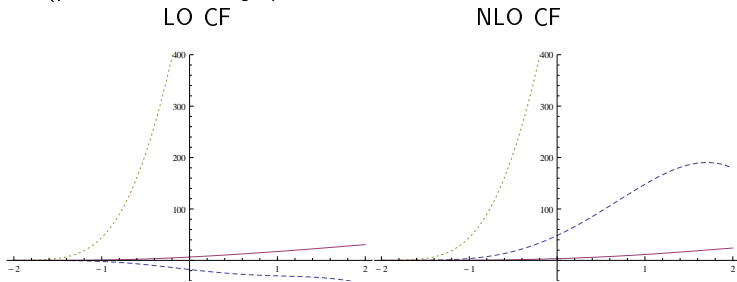


Figure:  $\frac{d\sigma}{dQ^2 dt dy d\phi}$  in  $pb/\text{GeV}^4$  for BH(dotted), TCS(solid), Interference(dashed) as a function of  $y$  (in CMS) for  $Q^2 = 4\text{ GeV}^2$ ,  $t = -0.1\text{ GeV}^2$ ,  $\phi = 0$ .

Case B (Pb beam on p target):

LO CF

NLO CF

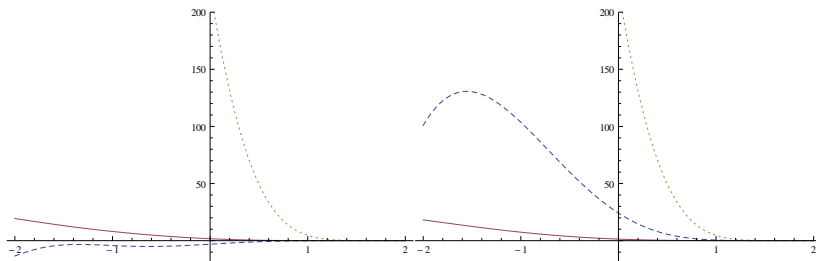
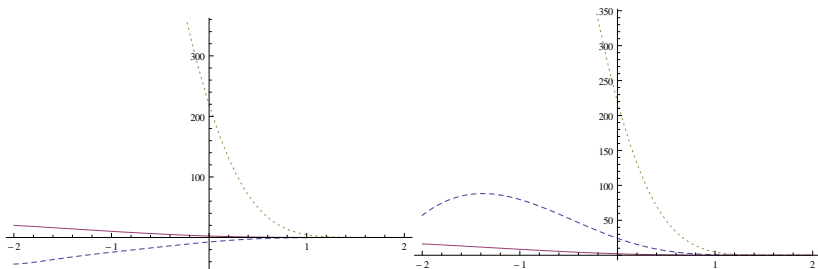


Figure:  $\frac{d\sigma}{dQ^2 dt dy d\phi}$  in  $pb/\text{GeV}^4$  for BH(dotted), TCS(solid), Interference(dashed) as a function of  $y$  (in CMS) for  $Q^2 = 4\text{GeV}^2$ ,  $t = -0.1\text{GeV}^2$ ,  $\phi = 0$ .

Case B (Pb beam on p target):

LO CF

NLO CF



**Figure:** Case 2 (Pb beam on p target):  $\frac{d\sigma}{dQ^2 dt dy d\phi}$  in  $pb/\text{GeV}^4$  for BH(dotted), TCS(solid), Interference(dashed) as a function of  $y$  (in CMS) for  $Q^2 = 4 \text{ GeV}^2$ ,  $t = -0.1 \text{ GeV}^2$ ,  $\phi = 0$ .

Case B (Pb beam on p target):

LO CF

NLO CF

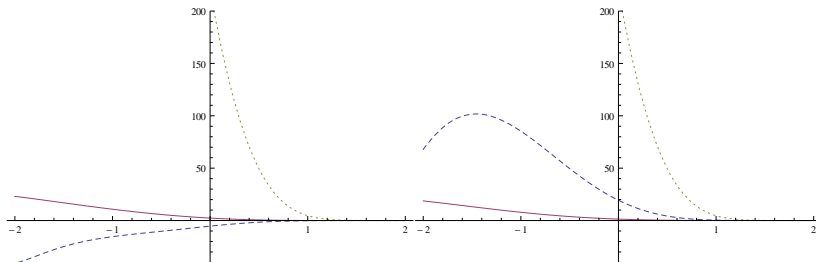


Figure: Case 2 (Pb beam on p target):  $\frac{d\sigma}{dQ^2 dt dy d\phi}$  in  $pb/GeV^4$  for BH(dotted), TCS(solid), Interference(dashed) as a function of  $y$  (in CMS) for  $Q^2 = 4 GeV^2$ ,  $t = -0.1 GeV^2$ ,  $\phi = 0$ .

## Summary

- TCS already measured in JLAB 6 GeV, but much richer and more interesting kinematical region available after upgrade to 12 GeV.
- Big NLO corrections from gluon sector,
- Better understanding of large terms is needed - factorization scheme? resummation ?
- Compton scattering in ultraperipheral collisions at hadron colliders opens a new way to measure generalized parton distributions
- TCS is an experimentally challenging study at JLab, COMPASS, RHIC and LHC, in many cases due to limitations of original detectors

## Summary

- TCS already measured in JLAB 6 GeV, but much richer and more interesting kinematical region available after upgrade to 12 GeV.
- Big NLO corrections from gluon sector,
- Better understanding of large terms is needed - factorization scheme? resummation ?
- Compton scattering in ultraperipheral collisions at hadron colliders opens a new way to measure generalized parton distributions
- TCS is an experimentally challenging study at JLab, COMPASS, RHIC and LHC, in many cases due to limitations of original detectors
- so we look forward for these studies at **AFTER@LHC**